Clays and Clay Minerals, Vol. 54, No. 4, 491–499, 2006.

STRUCTURAL AND CHEMICAL ALTERATION OF GLAUCONITE UNDER PROGRESSIVE ACID TREATMENT

MERVAT S. HASSAN* AND HASSAN M. BAIOUMY

Central Metallurgical R & D Institute, PO Box 87 Helwan, Cairo, Egypt

Abstract—Boiling glauconite from the El-Gideda area of Egypt in different concentrations of HCl and H_2SO_4 for different periods led to a modified structure. Treatment resulted in progressive destruction of the structure, leaving X-ray amorphous silica and only relics of the original mineral. The glauconitic material was modified structurally in order to increase its adsorption activity. The glauconite was evaluated in terms of mineralogy, chemistry, morphology, structural modification, octahedral cation leaching rate, surface area and cation exchange capacity using X-ray diffraction, infrared spectroscopy, X-ray fluorescence, scanning electron microscopy and surface area analysis. The ratio of extracted octahedral cations to the total octahedral cations in the untreated glauconite was taken as a measure of octahedral sheet decomposition. A progressive decrease in crystallinity and the formation of X-ray amorphous silica Si–O vibration bands at 1100, 800 and 494 cm^{-1} accompanied octahedral cation depletion. Acid activation using 2 M and 4 M HCl for 6 h destroyed 30% and 61% of the octahedral sheet, respectively. In contrast, similar treatment using 2.9 and 5.5 M H_2SO_4 destroyed 48% and 93% of the octahedral sheet, respectively. Depending on the extent of cation depletion, the 4 M HCl product surface areas were as high as 259 m^2/g, whereas the surface area of the 5.5 M H_2SO_4 product was only 63 m^2/g. The progressive increase in surface area was due to glauconite morphology alteration. Acid-induced dissolution of Al, Fe, Mg cations from octahedral sheet edges led to a wedge-like splitting of the glauconite crystals, mesopore creation, and greater access to interlayer galleries.

Key Words—El-Gideda, Egypt, Glauconite, Structural Modification.

INTRODUCTION

Glauconite is the dioctahedral Fe illite: $(K,Na)(Fe^{3+},Al,Mg,Fe^{2+})_2(Si,Al)_4O_{10}(OH)_2$. The structure of glauconite is essentially the same as muscovite and consists of dioctahedral T-O-T sheets. The octahedral sites usually contain more Fe^{3+} than Al^{3+} and significant amounts of Mg^{2+} and Fe^{2+} are common.

The structure usually contains variable amounts of expandable clay layers. Acid dissolution of many different clay minerals has been investigated as a means of preparing high-surface-area solids with properties well suited as adsorbents, catalysts and composite filling materials (Corma *et al*., 1987, 1990; Katunori *et al*., 1997; Balcı, 1996; Hymore, 1996; Dékány *et al*., 1999; Mervat *et al*., 1999; Vengris *et al*., 2001; Rompaey *et al*., 2002; Hongping *et al*., 2002).

The acid dissolution consists of: (1) removal of impurities; and (2) treatment with HCl, HNO_3 and H_2SO_4. The strong acids replace exchangeable cations (K^+, Na^+ and Ca^{2+}) by H^+ and some Al^{3+}, and partially extract Al, Fe and Mg from the 2:1 layer (Siddiqui, 1968). This treatment produces flat silicate layers with an extended surface useful for bleaching/refining of vegetable and mineral oils, and the reclamation of used lubricating oils, for example. The final reaction product of layer silicates upon acid treatment with H_2SO_4, HNO_3 and HCl was found to be an X-ray amorphous, porous, protonated and hydrated silica with a three-dimensional cross-linked structure (Siddiqui 1968; Komadel *et al*., 1990; Madejová *et al*., 1998; Rompaey *et al*., 2002). BET surface areas as great as 500 m^2/g have been reported for the X-ray amorphous silica derived from some of these minerals.

Data related to the chemical and structural changes and textural properties of glauconite following treatment with acid are very scarce in the literature; these aspects have only recently been studied (*e.g*. Srasra and Trabelsi-Ayed, 2000; Fernandez-Bastero *et al*., 2003; Mervat and El-Shall, 2004).

In this work, the structural modifications, increase in surface area, and general mechanism for the dissolution process in acid solutions have been examined by performing acid-leaching experiments on glauconite samples from the El Gideda area using several mineral acids, acid concentrations and activation times to produce materials with high added value to meet the strict specifications required for decolorization of vegetable oils and other industrial applications.

MATERIALS AND METHODS

Glauconitic materials for this study were collected from the El-Gideda area, Bahria Oasis, which forms an oval-shaped depression of ~15 km^2 in the central part of

* E-mail address of corresponding author:
mervathassan@hotmail.com
DOI: 10.1346/CCMN.2006.0540410

the Western Desert, ~370 km southwest of Cairo, Egypt. According to Mesead and Surour (1999), the glauconite facies of the El-Gideda mine area represents deposition in a shallowing-upward regime and consists of two large-scale cycles: (1) stratiform syndiagenetic glauconitic ironstone pockets and concretions predominating within the lower parts of the small-scale cycles; and (2) lateritic glauconitic ironstones, which formed during intermittent periods of subaerial weathering and lateritization of the parent glauconite facies.

The samples collected were examined for their mineralogy, chemical composition and petrography. A Philips PW 1730 X-ray generator with Fe-filtered CoKα run at 30 kV and 20 mA was used to examine both the bulk samples and the <2 μm clay fractions obtained using dispersion and sedimentation. The mixed layers in glauconite were measured from X-ray diffraction (XRD) patterns of the <2 μm fraction, following Weaver's (1956) method, using the positions of the resultant 001/001 (17 Å/10 Å) peaks after the ethylene glycol treatment.

Glauconite-rich samples were analyzed for their major elements using Philips X-ray fluorescence (XRF) equipment, PW 2404 operated at 40 kV and 60 mA, at the Geological Survey of Egypt. The vibrational spectra of the glauconite samples in KBr were recorded in Fourier transform mode using a Pye-Unicam SP 300 instrument at Cairo University. For each sample, 128 scans were recorded in transmittance mode over the 4000−400 cm^{-1} range, with a resolution of 4 cm^{-1}. The KBr pressed-disk technique (0.2 mg of sample and 200 mg of KBr) was used. The BET surface area was measured using a Quantachrome Nova 2000 Series device (Quantachrome Corporation of Syosset, New York), after degassing the samples overnight at 100ºC. The particle morphology and texture were observed by optical microscopy (Spot RT slider) and scanning electron microscopy (SEM with EDX) using a Japan Electron Optical Laboratories (JEOL) model 6335F scanning electron microscope, after coating the samples with Au-Pd.

The glauconite-rich sample was selected for modification under acid activation. The natural glauconite treated with HCl (2−4 M) and H_2SO_4 (2.9−5.5 M) solution at ~100ºC for 2, 4, 6 h. The activated samples were washed with water until pH 7 and dried at 90ºC and then evaluated using XRD, XRF, SEM with EDX and using the Nova 2000 Series device for measurement of the BET surface area.

RESULTS

Evaluation of the raw materials

Petrography. The samples examined were composed of green, pale-green, or yellowish-green to brownish-green grain-supported, highly-fractured glauconite pellets. The glauconite pellets had altered rims, which ranged from very fine-grained to coarse-grained, and were cemented by a pale-green to yellowish-green glauconitic matrix. The SEM images show glauconite platelets that are held apart by debris particles with many bent and curled crystals that form numerous mesopores (Figure 1a) and EDAX analysis shows that Si, Al, Fe and K are the major constituents (Figure 1b).

Mineralogy. The XRD pattern of glauconitic material is characterized by a low-angle, broad, glauconite diffraction peak (Figure 2). This XRD powder pattern is composed of *hk*0 and 001 broad and asymmetrical bands instead of discrete reflections, which may be related to the lack of three-dimensional periodicity

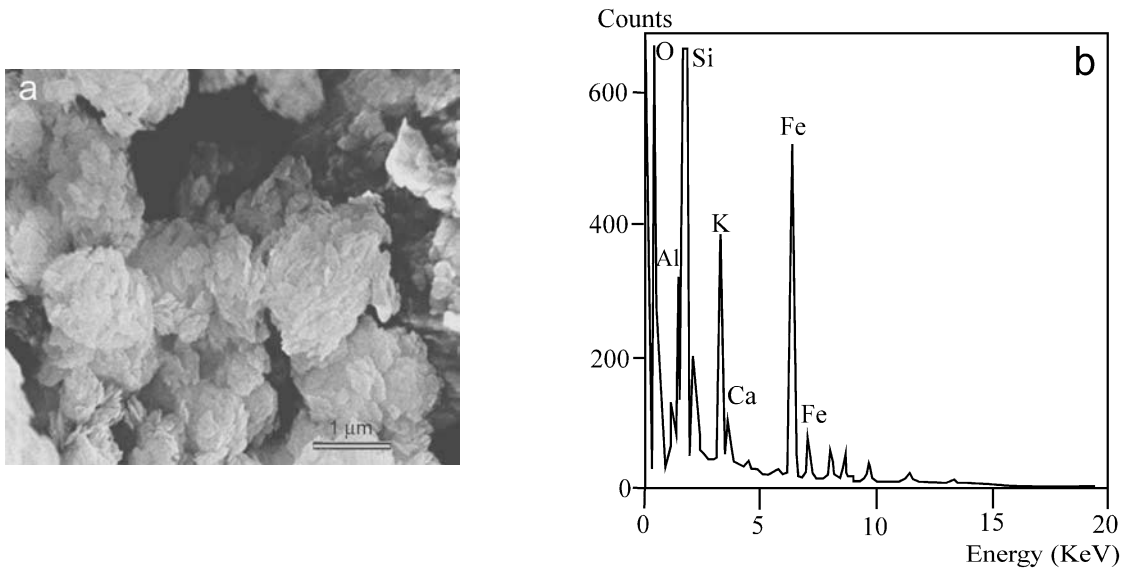

Figure 1. SEM image of glauconitic material (a) and EDX chemical analysis (b).

https://doi.org/10.1346/CCMN.2006.0540410 Published online by Cambridge University Press

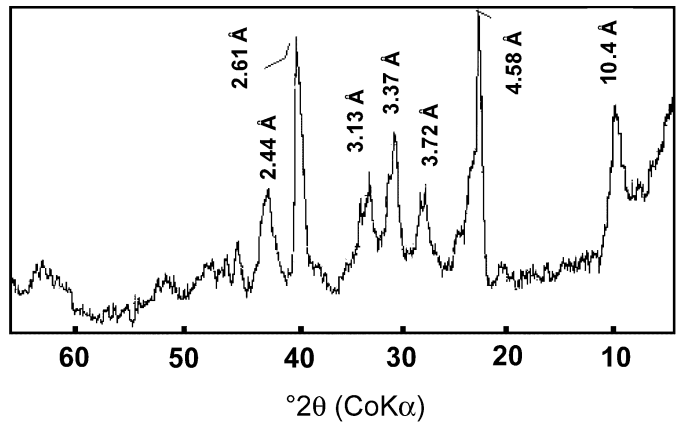

Figure 2. XRD pattern of glauconitic material.

because of random rotations or translations between layers, giving rise to extensive stacking disorder. Also, partial hydration of the sample can produce broadening of the basal reflections. The 112 and $1\bar{1}2$ reflections are broad and unresolved and several other reflections are also less well defined. According to Odom (1976), these diffraction characteristics indicate a disordered structure (1*Md*).

The XRD pattern of the <2 μm clay fraction (air dried and glycolated) is shown in Figure 3. Low-angle scattering ($\leqslant$9.8°2θ) is observed and may be produced by interlayer material in the sample. According to Thompson and Hower (1975), glauconite has the same complications as illite in that it may contain interstratified smectite layers. The term glauconite is usually used in a mineralogical sense to indicate an Fe-rich illite-smectite with all proportions of interlayering. After ethylene glycol solvation, the basal reflections broaden, especially at the base, and the diffraction effects spread between 8.1 and 10.4°2θ. According to Reynolds and Hower (1970), this glauconite sample contains <10% smectite layers and is described as *IMII* type.

The infrared (IR) spectra of glauconite material (Figure 4) have intense and complex bands (4000–400 cm^{-1}) that are in part due to hydroxyl groups and H_2O molecules.

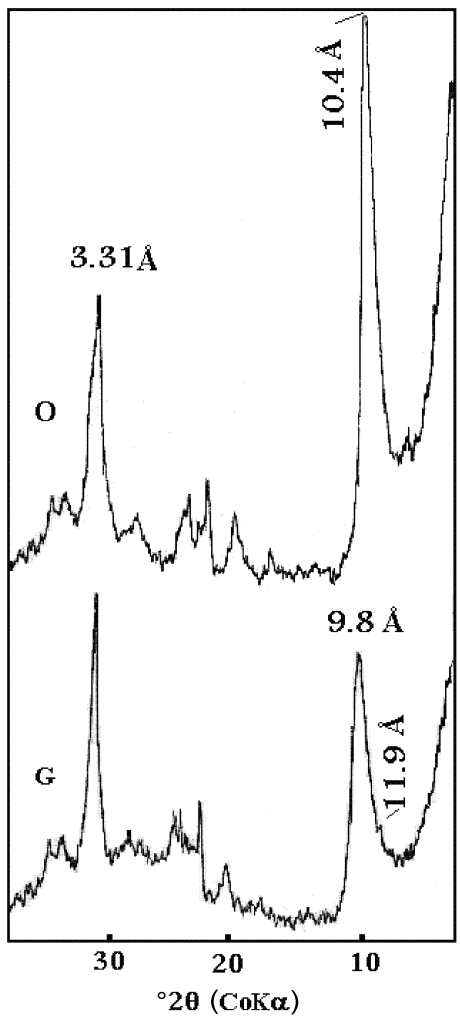

Figure 3. XRD pattern of an oriented <2 μm fraction.

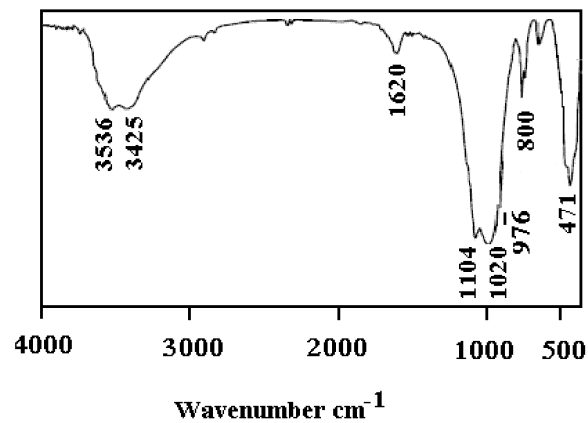

Figure 4. IR spectrum of glauconitic material.

https://doi.org/10.1346/CCMN.2006.0540410 Published online by Cambridge University Press

Spectra in the OH region show a broad, poorly resolved absorption band at 3536 cm^{-1}, which is assigned to the OH-stretching vibration in highly disordered glauconite (Figure 4). The broad band at 3425 cm^{-1} is attributed to the OH-stretching vibration of interlayer and hygroscopic H_2O. Absorption corresponding to the bending vibration of H_2O molecules occurs at 1620 cm^{-1} as a single band. In the lower-frequency region from 700 to 1200 cm^{-1}, the Si–O stretching absorption appears as two bands, at 1104 cm^{-1} for Si–O and at 1020 cm^{-1} for Si–O–Si. An unresolved band at 800 cm^{-1} is attributed to (Fe^{3+}MgOH and $Fe^{3+}Fe^{2+}$OH).

Chemical analysis. Chemical analysis of a representative glauconite sample indicated a very large SiO_2 content and large amounts of Fe_2O_3, K_2O and Al_2O_3. The other oxides, such as MgO, CaO and Na_2O were quite small.

Modified glauconitic structure

Effect of acid variation on the mineralogy of a representative sample. First we consider the acid dissolution of natural glauconite in 2 M and 4 M HCl. Under these conditions, the glauconite undergoes structural destruction due to dissolution of octahedral cations (Figure 5). The larger the dissolved fraction, the less crystalline the mineral becomes and the less intense its peaks appear on XRD patterns. For the first 2 h of the treatment, the changes in the XRD patterns were limited. After 4 h, however, there was a remarkable difference. The line intensities of almost all reflections, particularly that for the strongest line at 9.85°2θ, corresponding to the 10.4 Å reflection, decreased without significant change in peak position. For the samples treated for 6 h, there was still evidence of a weak glauconite pattern. The presence of a 001 reflection of glauconite confirmed that the glauconite structure was partially preserved. For the H_2SO_4 treatment, rapid dissolution of octahedral cations in the order 2.9 M H_2SO_4 < 5.5 M H_2SO_4, greatly diminished the XRD intensity. For the samples treated for 6 h, no crystallinity was visible after the 5.5 M H_2SO_4 treatment.

The different acid treatments changed the IR spectra of the glauconite samples (Figure 6). The most prominent change was the intensity reduction and then the disappearance of the OH-stretching band at ~3573 cm^{-1} with increased acidity and contact time with HCl. The tetrahedral sheet of the glauconite was also affected, especially at higher acid concentration. The Si–O–Si band at 1025 cm^{-1} decreased progressively, whereas the band at ~1100 cm^{-1} (assigned to the SiO_2 out-of-plane vibration) increased. This indicates that some siloxane Si–O–Si groups are destroyed by the acid activation and replaced by Si-OH groups. Meanwhile, treatment of glauconite with H_2SO_4 (2.9 and 5.5 M) increased the X-ray amorphous silica vibration band intensity at 1100 cm^{-1} and the intensities of the bands at 800 and 469 cm^{-1}, reflecting an alteration in the tetrahedral sheet with increasing acid concentration (Falaras *et al*., 1999). Madejová *et al*. (1998) used the decrease of the Si–O IR band at 1012 cm^{-1} and the intensity increase of the Si–O band for X-ray amorphous silica (near 1100 cm^{-1}) to quantify the extent of acid attack on hectorite.

Influence of acid nature, concentrations and leaching times on the final structure of glauconite. The effects of different acids, acid concentrations, and contact times on

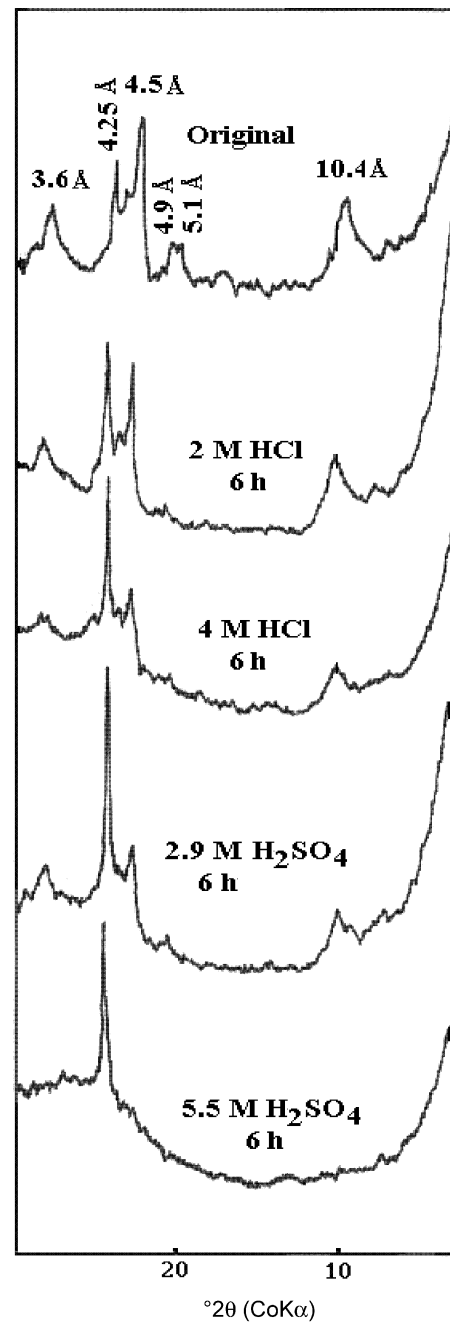

Figure 5. XRD patterns of glauconitic material before and after acid treatment.

https://doi.org/10.1346/CCMN.2006.0540410 Published online by Cambridge University Press

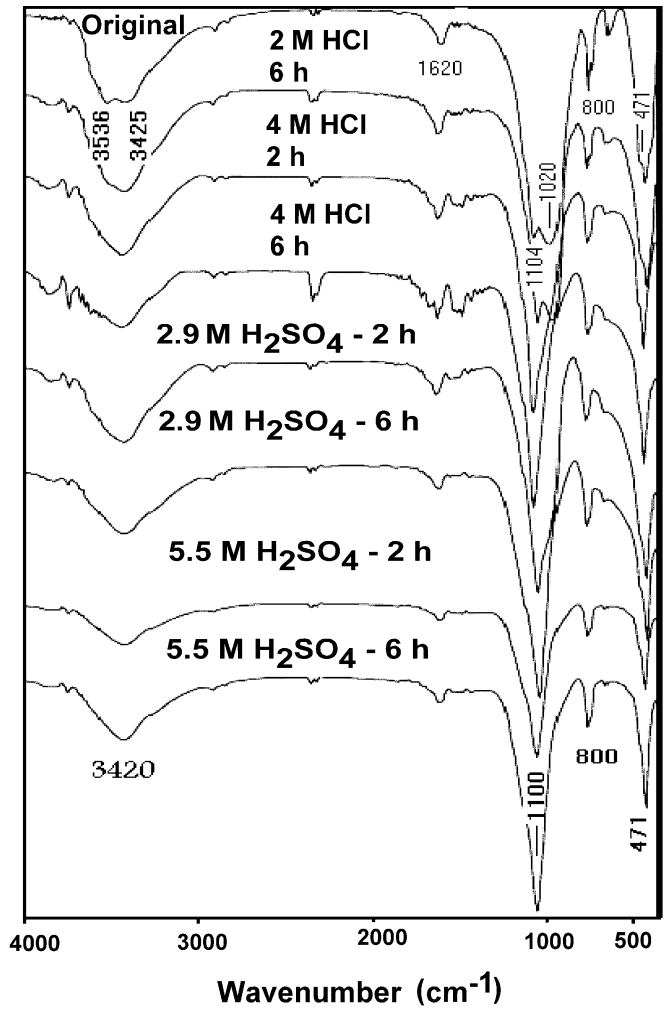

Figure 6. IR spectra of glauconitic material before and after acid treatment.

the leaching of Mg^{2+}, Al^{3+}, Fe^{3+} and K^{+} is shown in Figure 7. The ratio of extracted octahedral cations to the initial cations, $1-\alpha$, is taken as an indication of decomposition of octahedral sheets. It is well established that leaching of the octahedral cations provides clear evidence of the changes in glauconite composition following acid activation. The decrease in the octahedral sheet oxides (Al_2O_3, MgO, Fe_2O_3) along with the concomitant increase in silica content proved that the original structure was altered. It is clear that the amounts of the three cations leached increase in the order H_2SO_4 > HCl. Also, leaching of cations increased with increasing acid concentration as well as leaching times.

However, the extent of leaching is different at low concentrations of HCl (2 M) and H_2SO_4 (2.9 M); the Mg^{2+} is leached faster than Al^{3+} and Fe^{3+}. This indicates the order of removal of the octahedral ions from glauconite to be Mg > Fe > Al. A possible explanation is the influence of the cation-oxygen interaction. Al has the strongest interaction (E(Al-O) = 507.5 KJ mol^{-1}, E(Fe-O) = 408.8 KJ mol^{-1}, E(Mg-O) = 362.3 KJ mol^{-1}; Weast, 1984). The ratio of extracted octahedral cations to the total initial cations is taken as a measure of the decomposition of the octahedral sheet. Acid activation using 2 and 4 M HCl for 6 h destroyed 30% and 61% of the octahedral sheet, respectively. Meanwhile, 48% and 93% of the octahedral sheet was destroyed after treatment using 2.9 and 5.5 M H_2SO_4, respectively, for the same leaching time (Figure 8).

Effect of acid concentration and leaching time on surface area. In Figure 9, the BET surface areas of untreated and acid-treated glauconite samples are presented. The surface areas increase substantially from 20 m^2/g for the parent sample to values between 92 and 259 m^2/g in the modified samples, depending on the extent of depletion of the octahedral cations. It is noteworthy that the treatment of glauconite in 4 M HCl rather than 2 M HCl increases the surface area. Considerable changes of surface area observed during

https://doi.org/10.1346/CCMN.2006.0540410 Published online by Cambridge University Press

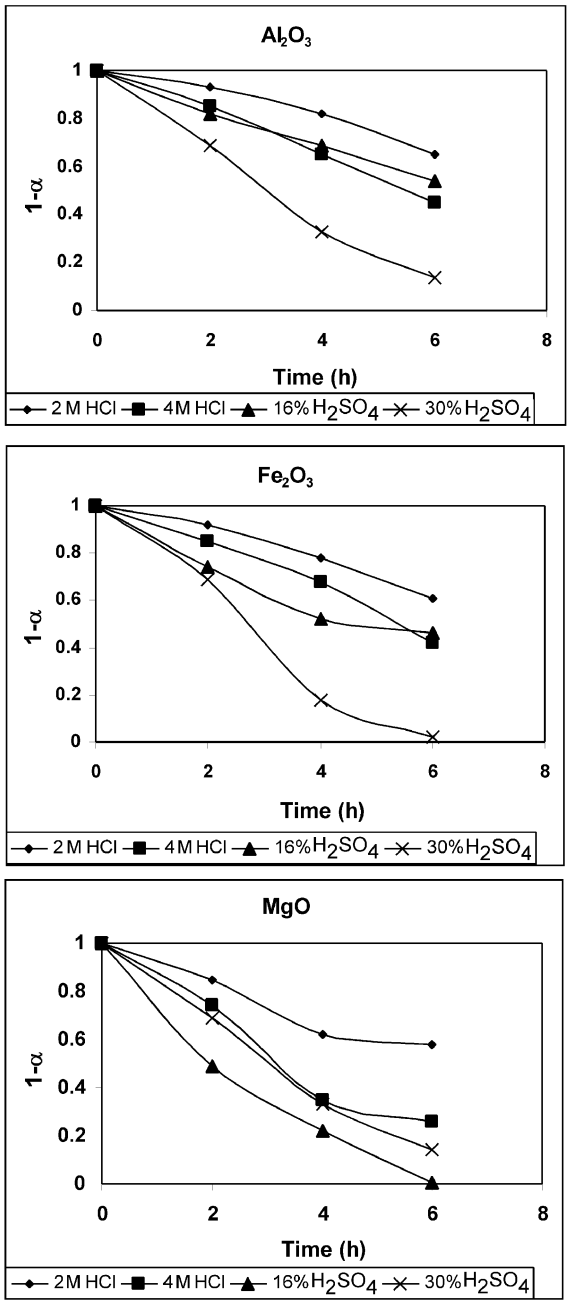

Figure 7. The relative amounts of leached oxides (1−α) after acid activation at different acid concentrations and different leaching times. (1−α = the ratio of extracted octahedral cations to the initial cations.)

modification of glauconite are caused by removal of octahedral cations and maximum surface area is achieved after removal of ~61% of the octahedral sheet. Thus, our results are in good agreement with previous reports on acid activation of glauconite (Srasra and Trabelsi-Ayed, 2000; Fernandez-Bastero *et al*., 2003), palygorskite (Corma *et al*., 1987), sepiolite (Vicente Rodriguez *et al*., 1994), and phlogopite and

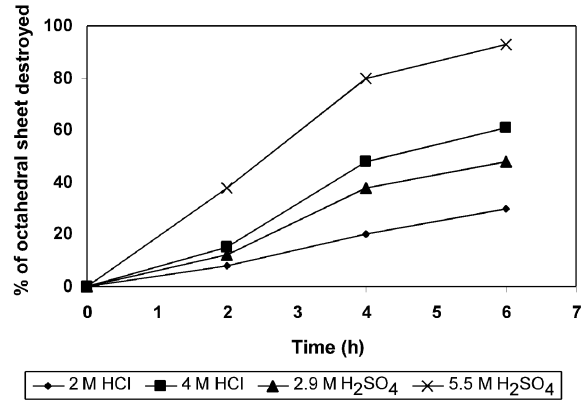

Figure 8. Ratio of decomposed octahedral sheets (%) as a function of acid concentration and leaching times.

fluorohectorite (Kaviratna and Pinnavaia, 1994). The crystallinity of the 2:1 structure decreases with acid treatment, whereas the BET surface area increases.

Treatment of glauconite in 5.5 M H_2SO_4 rather than 2.9 M H_2SO_4 reduced the surface area to the minimum value of 63 m^2/g. It is clear that 93% of octahedral cations were leached from the glauconite following acid activation by 5.5 M H_2SO_4 for 6 h. In parallel, relative silica content increased progressively and reached a maximum for the 5.5 M H_2SO_4, 6 h product. These observations agree with the IR and XRD data and correlate with the increase in the 800 cm^{-1} band for the silica and the appearance of a broad hump in the XRD pattern.

Mechanistic implication and significance. The acid dissolution of octahedral cations of glauconitic material is accompanied by the decrease in crystallinity as well as the formation of X-ray amorphous silica bands at 800 and 469 cm^{-1}. Nevertheless, the reaction products differ greatly in total surface area. Depending on the extent of acid dissolution, BET surface areas up to 259 m^2/g are found for 4 M HCl reaction products, whereas a surface

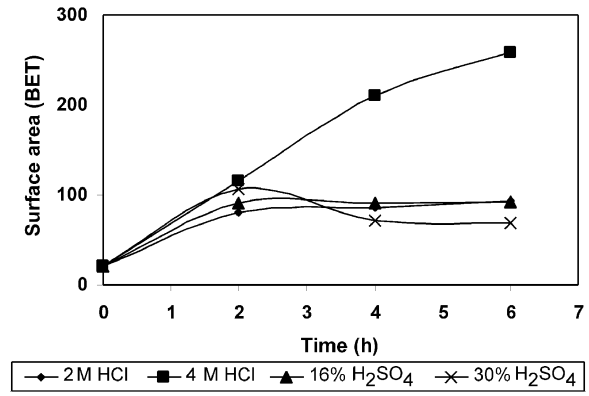

Figure 9. Nitrogen BET surface area of untreated and acid-leached glauconitic material.

https://doi.org/10.1346/CCMN.2006.0540410 Published online by Cambridge University Press

area of 63 m^2/g was found for the 5.5 M H_2SO_4 reaction product for the same contact time. These differences are attributed to the degree of depletion of glauconite octahedral cations using different mineral acids, acid concentrations and reaction times. We infer that the progressive increase in surface area is due to disturbance of the glauconite morphology (Fahn, 1979), and the acid-induced dissolution of Al, Fe, Mg cations from the edge of the octahedral sheet, leading to a wedge-like splitting of the glauconitic crystal. Attacking and crumbling some layers at their edges creates a considerable number of mesopores (Figures 10, 11).

The platelets of glauconite layers (Figure 10a) pile up, creating tectoid-like particles (Figure 10b); wedge-like splitting of glauconitic layers creates the open and mesopore structure shown in Figure 10c. Meanwhile, the gallery access is manifested at the later stages of octahedral cation depletion.

Increasing the reaction time to 6 h leads to greater depletion of Mg, Al and Fe from their structural positions, thereby allowing more hydrogen ions to diffuse into the open silicate structure. The gallery path may be facilitated by the structural disorder and reduction in layer charge density caused by proton edge attack or the edge-attack pathway becomes inhibited by the growing coating of silica at the edge sites (Kaviratna and Pinnavaia, 1994) (Figure 10).

DISCUSSION

Adsorption, catalytic ability and other industrial applications of clay minerals depend on their surface area, the amount and diameter of pores, as well as on specific properties of the surface. Particularly important are acidic properties of the surface related to the occurrence of acid centers of Bronsted and Lewis types. Clays, in general, have a large capacity for adsorbing organic compounds. Although bleaching earths are commonly based on montmorillonite, there appears to be no scientific basis for preferring this type of clay to others since the extensive interlayer surface of montmorillonite is not accessible to carotenoid molecules (Sarier and Guler, 1989). However, the high bleaching capacity of acid-activated montmorillonite clays may be ascribed to their large surface area most of which is contained in mesopores 2–10 nm in diameter that are accessible to the carotenoid pigments in vegetable oil.

For example, activated Fuller's earth (Tonsil optimum FF) has a surface area of 320 m^2/g and a mesopore volume of 0.38 m^2/g, whereas the respective values for the parent montmorillonite (before acid activation) are 65 m^2/g and 0.09 cm^3/g (Fahn, 1979). Likewise, acidic clays formed by a hydrothermal process in tuffaceous sediments and consisting essentially of montmorillonite can serve as effective decolorizing agents (Takeshi and Kato, 1969; Clarke, 1985). Also, some naturally acid clays of soil and hydrothermal origin in New Zealand, *e.g.* halloysite, kaolinite, montmorillonite and allophane (Theng and Wells, 1995) showed a relatively high propensity for decolorizing oil and butter. Meanwhile, their bleaching capacities required only minor treatment with HCl to optimize performance.

This finding opens the way for using local clays other than montmorillonite for bleaching purposes, *e.g.* Srasra and Trabelsi-Ayedi (2000) confirmed that the bleaching effect of Gafsa glauconite (Tunisia) on rapeseed oil was greatest when glauconite was activated for 4 h, and this correlates with the maximum external specific surface area achieved and the generation of strong acid sites.

With respect to the glauconitic materials of El Gideda, the remarkable change of surface and mineralogical properties upon activation can be characterized by the gradual breakdown of the glauconite crystal structure which is confirmed by XRD and IR. The complete breakdown of the glauconite structure by the formation of a so-called X-ray amorphous structure has been reported. From SEM images we infer that the increase in surface area is due to disturbance of the glauconite morphology (Bojemueller *et al.*, 2001) through attacking and crumbling some layers at the edges, leading to a wedge-like splitting of the glauconite

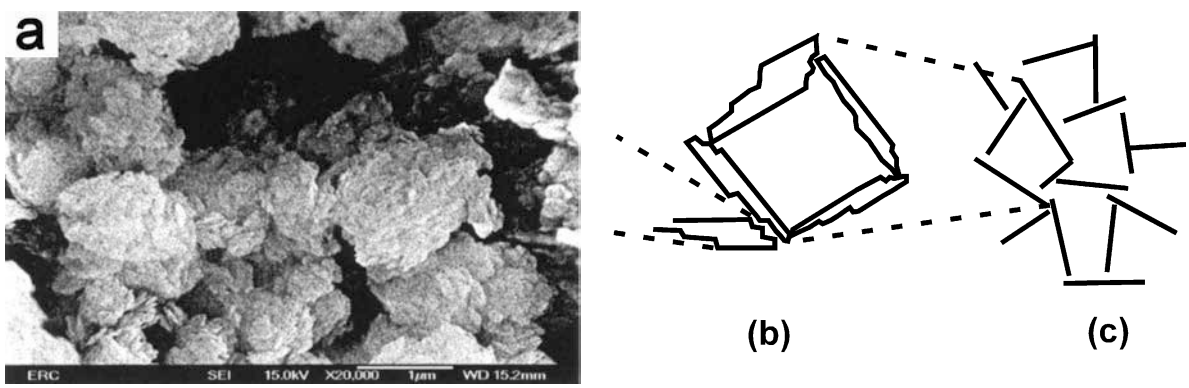

Figure 10. Generation of mesopore structure in glauconite after acid activation. (a) Platelets of glauconite; (b) wedge-like splitting of glauconite; (c) open mesopore structure.

https://doi.org/10.1346/CCMN.2006.0540410 Published online by Cambridge University Press

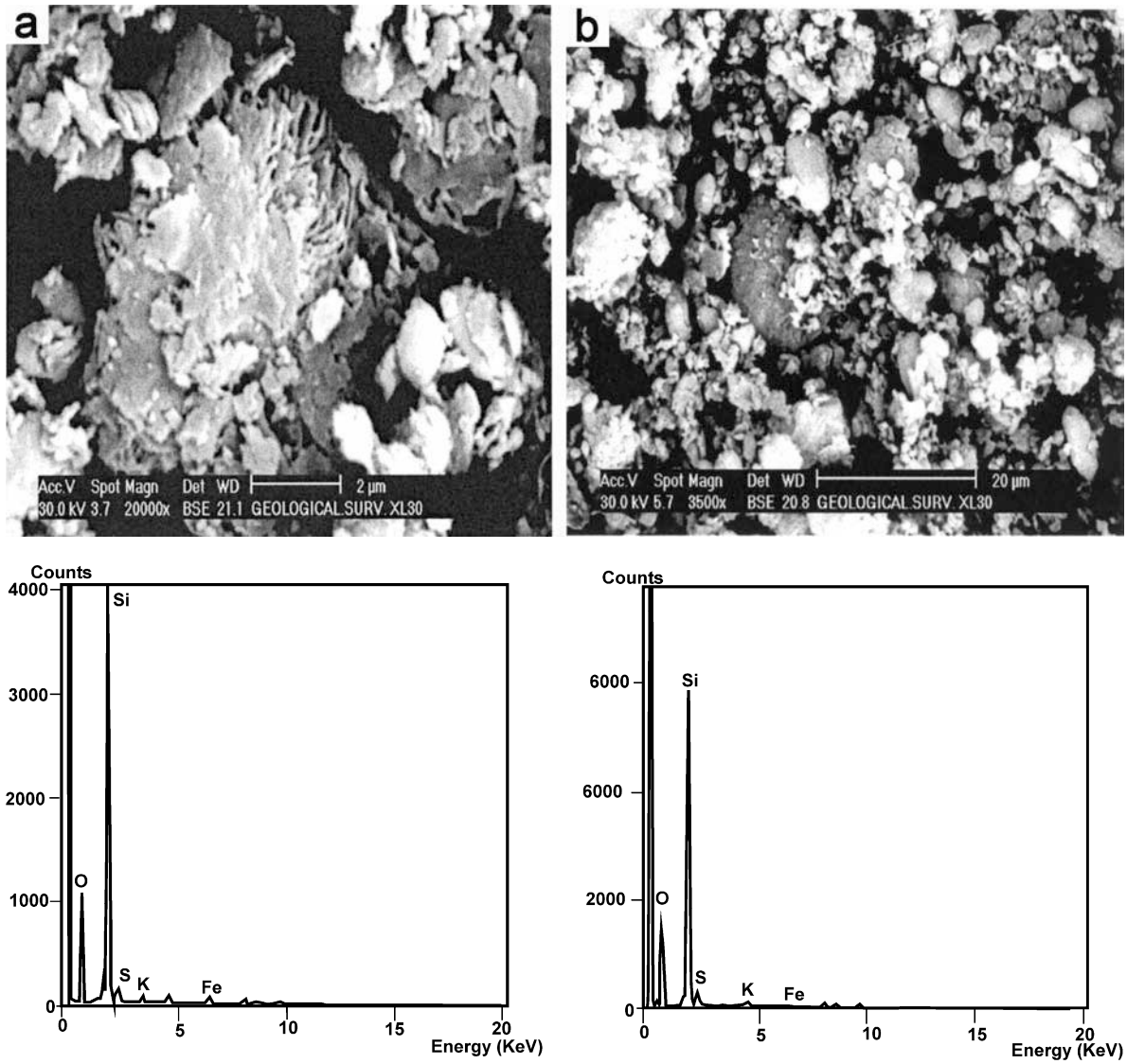

Figure 11. SEM image of glauconite and EDX chemical analyses: (a) 4 M HCl for 6 h; and (b) 5.5 M H_2SO_4 for 6 h.

crystal which creates considerable numbers of mesopores and increases the mesopore volume (Mervat and El-Shall, 2004). The stripping of Al^{3+}, Fe^{3+} and Mg^{2+} from the octahedral sheet, (together with OH) and Si^{4+}, results in an increase in charge in the structure. For electrical neutrality, the surface of the layered silicate will adsorb H^+ to form Lewis acid sites capable of drawing electrons and consequently improving the capacity for bleaching and adsorption with this modified structure.

On the other hand, the surface acidity of the modified glauconite structure, together with the formation of X-ray amorphous colloidal silica (Fahn, 1979) could improve the sorption capacity of this structure. The colloidal silica (gel) that formed during acid activation of clay minerals would provide additional surface area. Further, Bronsted acid sites, the concentration of which increases appreciably on activation (Morgan *et al*., 1985; Theocharis *et al*., 1988), are apparently associated with silanol groups in the silica gel structure as we can see from IR spectra of the glauconite studied.

CONCLUSIONS

(1) Acid activation of glauconitic material from the El-Gideda area produces an increase in the specific surface area.

(2) With the variables considered (acid type, acid concentration and treatment time) and in the ranges used, the maximum specific surface area was obtained from treatment with 4 M HCl for 6 h.

(3) Acid activation disturbs the original morphology of glauconite aggregates, resulting in loosening of the structure through depletion of octahedral cations.

https://doi.org/10.1346/CCMN.2006.0540410 Published online by Cambridge University Press

(4) Prolonged and stronger activation results in the transformation of glauconite into an X-ray amorphous substance with granular structure, similar to forms of silica gels. The formation of this substance has been demonstrated by XRD and IR spectroscopy.

ACKNOWLEDGMENTS

We acknowledge Dr Ibrahim Ahmed, head of the hydrometallurgy laboratory at the Central Metallurgical R&D Research Institute, Cairo, for his help with the acid-activation treatment of the glauconite investigated.

REFERENCES

Balcı, S. (1996) Thermal decomposition of sepiolite and variations in pore structure with and without acid pre-treatment. *Journal of Chemical Technology and Biotechnology*, **66**, 72– 78.

Bojemueller, E., Nennemann, A. and Lagaly, G. (2001) Enhanced pesticide adsorption by thermally modified bentonites. *Applied Clay Science*, **18**, 277–284.

Clarke, G.H. (1985) Special clays. *Industrial Minerals*, **216**, 25–51.

Corma, A., Mifsud, A. and Sanz, E. (1987) Influence of the chemical composition and textural characteristics of palygorskite on the acid leaching of octahedral cations. *Clay Minerals*, **20**, 13–27.

Corma, A., Mifsud, A. and Sanz, E. (1990) Kinetics of the acid leaching of palygorskite: Influence of the octahedral sheet composition. *Clay Minerals*, **25**, 197–205.

Dékány, I., Turi, L., Fonseca, A. and Nagy, J.B. (1999) The structure of acid treated sepiolites: small angle X-ray scattering and multi MAS-NMR investigations. *Applied Clay Science*, **14**, 141–160.

Fahn, R. (1979) Acid activated clays and their adsorption properties. *Proceedings of the Society of Mining and Engineers, AIME, Tucson, Arizona*, **79**, 1–13.

Falaras, P., Kovanis, I., Lezou, F. and Seiragakis, G. (1999) Cottonseed oil bleaching by acid activated montmorillonite. *Clay Minerals*, **34**, 221–232.

Fernandez-Bastero, S., Garcia, T., Santos, A. and Gago-Duport, L. (2003) Structural and compositional variation in glauconites from acid dissolution process at low temperature. *Journal of Geophysical Research Abstract*, **5**, 14353.

Hongping, H., Jiugao, G., Xiande, X., Hongfu, L. and Liyun, L. (2002) A microstructural study of acid-activated montmorillonite from Choushan, China. *Clay Minerals*, **37**, 337–349.

Hymore, F.K. (1996) Effects of some additives on the performance of acid-activated clays in the bleaching of palm oil. *Applied Clay Science*, **10**, 379–385.

Katunori, K., Koji, S. and Atsumu, T. (1997) Advanced utilization of serpentine, preparation and utilization of amorphous siliceous materials from serpentine ($Mg_2Si_2O_5(OH)_4$) by acid treatment. *Report of the National Institute for Resources and Environment*, **18**.

Kaviratna, H. and Pinnavaia, T.J. (1994) Acid hydrolysis of octahedral Mg^{2+} sites in 2:1 layered silicates: An assessment of edge attack and gallery access mechanisms. *Clay Minerals*, **42**, 717–723.

Komadel, P., Schmidt, D., Madejová, J. and Čičel, B. (1990) Alteration of smectites by treatments with hydrochloric acid and sodium carbonate solutions. *Applied Clay Science*, **5**, 113– 122.

Madejová, J., Bujdák, J., Janek, M. and Komadel, P. (1998) Comparative FT-IR study of structural modifications during acid treatment of dioctahedral smectites and hectorite. *Spectrochimica Acta*, **54**, 1397–1406.

Mervat, S.H. and El-Shall, H. (2004) Glauconitic clay of El Gidida, Egypt. Evaluation and surface modification. *Applied Clay Science*, **27**, 219–222.

Mervat, S.H., Ismael S.I. and Ibrahim, A.I. (1999) Aspects of modification of the structure and decolorizing power of Egyptian Fullers Earth. *Erzmetall*, 579–583.

Mesaed, A.A. and Surour, A.A. (1999) Mineralogy and geochemistry of the Bartonian strata bound diagenetic and lateritic glauconitic ironstones of El-Gidida mine, Bahria Oasis, Egypt. *International Conference on Geology of the Arab World, Cairo University , Egypt*, 509–540.

Morgan, D.A., Shaw, D.B., Sidebottom, M.I., Soon, T.C. and Taylor, R.S. (1985) The function of bleaching earths in the processing of palm kernel and coconut oils. *Journal of the American Oil Chemical Society*, **62**, 292–299.

Odom, E. (1976) Microstructure, mineralogy and chemistry of Cambrian glauconite pellets and glauconite, Central USA. *Clays and Clay Minerals*, **24**, 232–238.

Reynolds, R.C. and Hower, J. (1970) The nature of interlayering in mixed-layer illite-montmorillonites. *Clays and Clay Minerals*, **18**, 25–36.

Rompaey, K.V., Van Ranst, E., De Coninck, F. and Vindevogel, N. (2002) Dissolution characteristics of hectorite in inorganic acids. *Applied Clay Science*, **2**, 241–256.

Sarier, N. and Guler, C. (1989) The mechanism of β-carotene adsorption on activated montmorillonite. *Journal of the American Oil Chemical Society*, **66**, 917–923.

Siddiqui, M.K.H. (1968) *Bleaching Earths*. Pergamon, Oxford, UK, 68 pp.

Srasra, E. and Trabelsi-Ayedi, M. (2000) Textural properties of acid-activated glauconite. *Applied Clay Science*, **17**, 71–84.

Takeshi, H. and Kato, C. (1989) Montmorillonite minerals. Pp. 103–120 in: *The Clays of Japan.* Geological Survey of Japan, Tokyo.

Theng, B.K.G. and Wells, N. (1995) Assessing the capacity of some New Zealand clays for decolorizing vegetable oil and butter. *Applied Clay Science*, **9**, 321–326.

Theocharis, C.R., Jacob, K.J. and Gray, A. (1988) Enhancement of Lewis acidity in layer aluminosilicates. *Journal of the Chemical Society, Faraday Transactions*, **84**, 1509–1516.

Thompson, G.R. and Hower, J. (1975) The mineralogy of glauconite. *Clays and Clay Minerals*, **23**, 289–300.

Vengris, T., Binkiene, R. and Sveikauskaite, A. (2001) Nickel, copper and zinc removal from waste water by a modified clay sorbent. *Applied Clay Science*, **18**, 183–190.

Vicente Rodriguez, M.A., Lopez Gonzalez, J.D. and Banares Munoz, M. (1994) Acid activation of a Spanish sepiolite: physicochemical characterization, free silica content and surface area of products obtained. *Clay Minerals*, **29**, 361–367.

Weast, R.C. (1984) *Handbook of Chemistry and Physics*, 65th edition. CRC Press, Boca Raton, Florida.

Weaver, C.E. (1956) The distribution and identification of mixed-layer clays in sedimentary rocks. *American Mineralogist*, **41**, 202–221.

(*Received 2 November 2004; revised 24 February 2006; Ms. 976; A.E. William F. Jaynes*)